LOW COMPLEXITY SIMULATION OF WIRELESS CHANNELS USING DISCRETE PROLATE SPHEROIDAL SEQUENCES

Florian Kaltenberger[1], *Thomas Zemen*[2], *Christoph W. Ueberhuber*[3]

[1]Corresponding Author:
F. Kaltenberger
ARC Seibersdorf research GmbH
Donau-City-Str. 1,
1220 Vienna, Austria
E-mail:
florian.kaltenberger@arcs.ac.at

[2]Forschungszentrum
Telekommunikation Wien
Donau-City-Str. 1,
1220 Vienna, Austria
E-mail: thomas.zemen@ftw.at

[3]Vienna University of Technology
Wiedner Hauptstrasse 8-10/101
1040 Vienna, Austria
E-mail:
c.ueberhuber@tuwien.ac.at

Abstract The modeling and simulation of wireless mobile communication channels is very important for the design and testing of receiver algorithms. Especially for the testing of mobile radio hardware devices, real-time implementations of such channel models are required.

This work presents a low-complexity algorithm for the simulation of time-variant flat-fading channels. The new method is based on a subspace representation of the channel transfer function. We develop an algorithm to calculate the projection on this subspace in $\mathcal{O}(1)$ operations. By adjusting the dimension of the subspace it is possible to trade complexity for accuracy.

We analyze an implementation on a digital signal processor with a 16 bit fixed-point arithmetic. The computational complexity can be reduced by one order of magnitude compared to a conventional sum-of-sinusoids implementation.

1. Introduction

The wireless radio channel can be modeled as a linear time-variant system. This system is uniquely characterized using a time-variant impulse response $h(t,\tau)$ where t denotes time and τ denotes the time delay of the impulse response. Complex symbols are transmitted over the channel at rate $1/T_\mathrm{S}$. If the symbol duration T_S is much longer than the support of the impulse response T_D, the channel is called *frequency-flat*. In contrast to block fading channels, where the impulse response is assumed to be constant over a certain time, *time-variant* channels change from symbol to symbol.

Looking at the far field only, and assuming plane waves which are scattered at objects, the time-variant flat-fading channel is modeled as a superposition of different propagation paths using ray tracing principles (see Figure 1). Thus we avoid the complexity of a general solution of Maxwell's equations. The time-variant characteristic of the flat-fading channel depends on the placement of the scattering objects and the user's velocity. A special case is the scatterer placement on a circle around the receiver, which is usually known as Jakes model [1, 2]. A more general model would be a geometry based stochastic channel model as described in [3, 4].

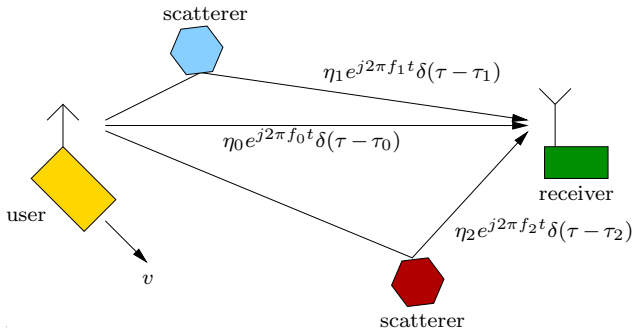

Figure 1: Time-variant multi-path propagation model for a wireless radio channel. The signals sent from the transmitter, moving at speed v, arrive at the receiver. Each path p has attenuation η_p, time delay τ_p and Doppler shift f_p

Such a channel model has a high computational complexity, because for every propagation path and every time instance a complex exponential has to be evaluated. On a real-time hardware channel simulator, like the *ARC SmartSim* [5], the number of paths P, that can be simulated, is limited by the available processing power. In this paper, a new method is introduced, that allows both to increase the number of paths P and to reduce the overall computational complexity.

To achieve this goal, we make the following important observations. Firstly, in typical wireless communication channels the maximum variation of the channel in time, measured using the (one sided) normalized Doppler bandwidth ν_{Dmax}, is much smaller than the available normalized channel bandwidth. Thus, the time-variant channel is highly oversampled, or in other words

$$\nu_{\mathrm{Dmax}} \ll 1/2. \tag{1}$$

Secondly, the channel simulation will be performed for a predefined time-interval M.

Slepian [6] showed, that the subspace of $\ell^2(\mathbb{Z})$, that contains all bandlimited sequences with bandwidth ν_{Dmax}, whose energy is concentrated on the index set $\{0,\ldots,M-1\}$, is spanned by the discrete prolate spheroidal (DPS) sequences

$$v_m^{(d)}(M,\nu_{\mathrm{Dmax}}), \quad d=0,\ldots,D'-1. \tag{2}$$

The essential dimension of the subspace is given by $D' = \lceil 2\nu_{\mathrm{Dmax}} M \rceil + 1$. For typical wireless communication systems this dimension is extremely small due to the high oversampling (1). This basic observation is the foundation of the new subspace based channel simulation, which is outlined in the next section.

Our contributions in this paper are:

- Applying the subspace representation of a time-variant channel from [7] to time-variant channel *simulation*.
- Introducing the approximate DPS wave functions to calculate the projection on the subspace in $\mathcal{O}(1)$ operations.
- Providing a detailed error and complexity analysis that allows to trade efficiency for accuracy.

The paper is organized as follows. In Section 2, the signal model is introduced. Section 3 gives an overview of a channel simulator, that is used as a target platform. In Section 4, the discrete prolate spheroidal sequences are reviewed. In Section 5 the subspace representation is introduced, while in Section 6 the calculation of the coefficients of this basis representation is shown. Finally we give a detailed error and complexity analysis of the algorithm in Section 7 and draw conclusions in Section 8.

2. Signal Model

We model the sampled time-variant frequency-flat channel

$$h_m := \int h(mT_S, mT_S - \tau) d\tau \tag{3}$$

as superposition of P individual propagation paths, (see Fig. 1):

$$h_m = \sum_{p=0}^{P-1} \eta_p e^{j2\pi f_p m T_s} = \sum_{p=0}^{P-1} \eta_p e^{j2\pi \nu_p m}, \tag{4}$$

where m denotes discrete time, and η_p and $\nu_p = f_p T_S$ are the complex attenuation and the normalized Doppler shift of path $p = 0,\ldots,P-1$ respectively. Further, we assume that the energy of every path is $\mathcal{E}\{|\eta_p|^2\} = 1/P$.

The system description of such a time-variant frequency-flat radio channels simplifies to

$$y_m = h_m x_m + n_m, \tag{5}$$

with $x_m, y_m \in \ell^2(\mathbb{Z})$ are the discrete, finite energy input and output signals respectively and n_m is a sequence of independent identically distributed (i.i.d.) random variables drawn from a circular symmetric complex Gaussian distribution with zero mean and variance N_0.

The maximum variation of h_m in time is upper bounded by the maximum (one sided) normalized Doppler bandwidth ν_{Dmax},

$$|\nu_p| \le \nu_{\mathrm{Dmax}} = \frac{v_{\max} f_C}{c} T_S, \quad p=0,\ldots,P-1, \tag{6}$$

where $v_{\max}$ is the maximum velocity of the user, f_C is the carrier frequency, and c denotes the speed of light [4].

3. Real Time Channel Simulation

In a real-time channel simulator, like the *ARC SmartSim* [5], Equations (4) and (5) have to be evaluated on-line at every time instance m.

The hardware of the channel simulator is a parallel architecture of digital signal processors (DSPs) and field programmable gate arrays (FPGAs). While the convolution of the channel with the input signal is done in the FPGA, the calculation of the channel h_m (4) is done in the DSP.

The DSP has a fixed point architecture with 16 bit precision. In such an architecture, the evaluation of the complex exponential in (4) is quite costly and is usually done using table look-up and interpolation. In [5] for example, we use a table with 8 bit precision and a linear interpolation for values in between the table entries. This implementation needs 6 additions, 4 multiplications and 2 memory accesses.

4. The discrete prolate spheroidal sequences

In this section, the most important results of [6] are reviewed. Slepian [6] asked, which sequences $v_m \in \ell^2(\mathbb{Z})$ are bandlimited, i. e. whose Fourier transform $V(f)$ vanishes outside a given interval $[-\nu_{\mathrm{Dmax}}, \nu_{\mathrm{Dmax}}]$,

$$V(f) = \sum_{m=-\infty}^{\infty} v_m e^{2\pi j m f}, \tag{7}$$

$$v_m = \int_{-\nu_{\mathrm{Dmax}}}^{\nu_{\mathrm{Dmax}}} V(f) e^{-2\pi j m f} df \tag{8}$$

and whose energy concentration on the interval $m \in \{0, \ldots, M-1\}$ is maximal

$$\lambda = \frac{\sum_{m=0}^{M-1} |v_m|^2}{\sum_{m=-\infty}^{\infty} |v_m|^2} \to \max. \tag{9}$$

The solutions to this problem are given by the discrete prolate spheroidal (DPS) sequences

$$v_m^{(d)} = v_m^{(d)}(M, \nu_{\mathrm{Dmax}}),\ d = 0, \ldots, M-1, \tag{10}$$

which are defined as the solutions of the eigenvalue problem

$$\sum_{n=0}^{M-1} \frac{\sin 2\pi \nu_{\mathrm{Dmax}}(m-n)}{\pi(n-m)} v_n^{(d)} = \lambda_d v_m^{(d)}. \tag{11}$$

The corresponding eigenvalues

$$\lambda_d = \lambda_d(M, \nu_{\mathrm{Dmax}}),\ d = 0, \ldots, M-1 \tag{12}$$

denote to the actual time concentration of the sequence. The eigenvalues λ_d are clustered around 1 for $d < D'$, and decay exponentially for $d > D'$, where $D' = \lceil 2M\nu_{\mathrm{Dmax}} \rceil + 1$ is the essential dimension of the signal subspace. The DPS sequences are doubly orthogonal on the index set $\{0, \ldots, M-1\}$ and on $\mathbb{Z}$.

5. Subspace Representation

In this section, a subspace representation of the channel model (4) is introduced. Using the observations made in Section 1 and the results of the previous section, we chose the subspace to be the one spanned by the first D DPS sequences

$$S = \mathrm{span}\{v_m^{(d)}(M, \nu_{\mathrm{Dmax}}), d = 0, 1, \ldots, D-1\}. \tag{13}$$

The parameters M and ν_{Dmax} depend on the oversampling factor OSF:

$$M = M_C \cdot \mathrm{OSF} \tag{14}$$

$$\nu_{\mathrm{Dmax}} = f_{\mathrm{Dmax}} \cdot T_S = f_{\mathrm{Dmax}} \cdot \frac{T_C}{\mathrm{OSF}}, \tag{15}$$

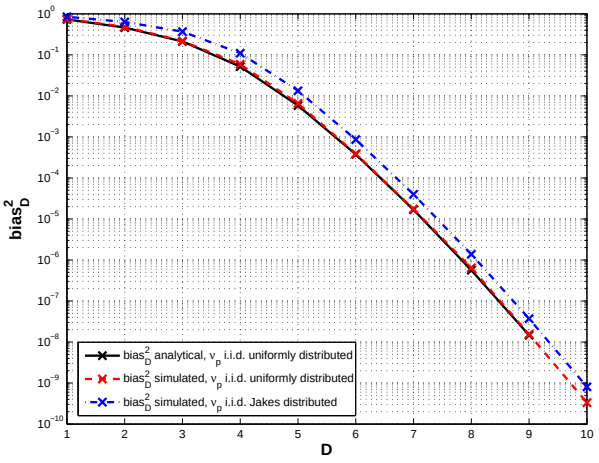

Figure 2: Bias of the subspace representation of the channel. The results of the single-path model as well for the multi-path model were evaluated numerically for the case that the ν_l are uniformly distributed and distributed according to the Jakes model respectively. Also the theoretical bound (19) is plotted as a reference.

where M_C is the blocklength in chips and T_C is the duration of a chip. Unless otherwise stated, the parameters M, ν_{Dmax}, and OSF stay the same for the whole simulation and we drop the explicit dependence of the DPS sequences $v_m^{(d)}(M, \nu_{\mathrm{Dmax}})$ on them.

Projecting $h_m,\ m \in \{0, \ldots, M-1\}$ onto S, we obtain

$$\hat{h}_m = \sum_{d=0}^{D-1} \alpha_d v_m^{(d)}. \tag{16}$$

The basis coefficients α_d of (16) are obtained by projecting the transfer function of each single-path p onto S:

$$\gamma_{d,p} = \sum_{m=0}^{M-1} e^{j2\pi\nu_p m} v_m^{(d)}, \tag{17}$$

and summing them up

$$\alpha_d = \sum_{p=0}^{P-1} \eta_p \gamma_{d,p}. \tag{18}$$

The mean square error or square bias of the subspace representation (16) is defined as

$$\mathrm{bias}_D^2 = \mathcal{E}\left\{ \frac{1}{M} \sum_{m=0}^{M-1} |h_m - \hat{h}_m|^2 \right\}, \tag{19}$$

where $\mathcal{E}\{\cdot\}$ denotes expectation with respect to the Doppler shifts ν_p. As shown in the Appendix, the square bias of the multi-path model can be upper bounded by the square bias of the single path model, if it is assumed that the Doppler shifts ν_p as well as the attenuations η_p, $p = 0, \ldots, P-1$ are independently distributed. Therefore, the upper bound of the square bias does not depend on the number of simulated paths.

The square bias depends not only on the subspace dimension D, but also on the distribution of the Doppler shifts. In Figure 2, the square bias is plotted for Doppler shifts drawn from a uniform distribution as well as from a Jakes distribution. Also, the analytical square bias for the uniform distribution, which is derived in the Appendix, is plotted.

The simulation results were obtained using the parameters of an UMTS high speed downlink packet access system (HSDPA) [8], which are summarized in Table 1. The oversampling factor (OSF) is chosen in accordance with the parameters of the hardware channel simulator in [5]. The maximum normalized Doppler frequency $\nu_{\mathrm{Dmax}} = 7.5352 \cdot 10^{-6}$.

Parameter	Value
Oversampling factor OSF	32
Sample time T_S	$3.84 \cdot 10^{-6} \cdot \mathrm{OSF}^{-1}$ sec
Blocklength M	$7680 \cdot \mathrm{OSF}$ samples
No. paths P	20
Carrier frequency f_c	$2 \cdot 10^9$ Hertz
Mobile velocity $v_{\max}$	500 kmph

Table 1: Simulation parameters for the numerical experiments.

It can be observed, that the square bias of the subspace representation decays exponentially with the subspace dimension. The analytical square bias gives a good match, in the case that the Doppler shifts are uniformly distributed. In case of a Jakes distribution, the square bias is slightly shifted to the right, but has the same exponential decay.

The analysis and simulations show, that the dimension D of the subspace can be adjusted according to the required numerical precision. For example, in a fixed-point implementation with 16 bits precision, the maximum achievable numerical precision is $2^{-15} \approx 3 \cdot 10^{-5}$. For the parameters of the example above, this would require a subspace dimension of $D = 7$. We make the important note, that the required subspace dimension is *independent* of the number of propagation paths P.

The key result of this paper is, that the projection (17) can be calculated in $\mathcal{O}(1)$ operations, as it will be shown in the next section. Thus, the need of evaluating the complex exponentials for calculating h_m has been eliminated.

6. Calculation of the basis coefficients

To calculate the basis coefficients $\gamma_{d,p}$, we take advantage of the DPS wave functions $U_d(f)$, which are the amplitude spectra of the DPS sequences $v_m^{(d)}$. Slepian [6] showed that the amplitude spectrum of a DPS sequence limited to $m \in \{0, \dots M-1\}$ is a scaled version of the associated DPS wave function (cf. (26) in [6])

$$U_d(f) = \epsilon_d \sum_{m=0}^{M-1} v_m^{(d)} e^{-j\pi(M-1-2m)f}, \tag{20}$$

where $\epsilon_d = 1$, if d even, and $\epsilon_d = j$ if d odd.

Comparing (17) with (20) shows that the basis coefficients can be calculated according to

$$\gamma_{d,p} = \gamma_d(\nu_p) = \frac{1}{\epsilon_d} e^{j\pi(M-1)\nu_p} U_d(\nu_p). \tag{21}$$

The following definition and theorem show that $U_d(\nu_p)$ can be approximately calculated from $v_m^{(d)}$ by a simple scaling and shifting operation.

Definition 6.1 *Let $v_m^{(d)}$, $d = 0, \dots, M-1$ be the DPS sequences with (normalized) bandwidth ν_{Dmax} and block length M. Further let λ_d, $d = 0, \dots, M-1$ denote the corresponding eigenvalues. We define* approximate DPS wave functions *as*

$$\tilde{U}_d(\nu_p) := \pm \sqrt{\frac{\lambda_d M}{2\nu_{Dmax}}} v^{(d)}_{m(\nu_p/\nu_{Dmax})}, \tag{22}$$

where

$$m\left(\frac{\nu_p}{\nu_{Dmax}}\right) = \left\lfloor \left(1 + \frac{\nu_p}{\nu_{Dmax}}\right) \frac{M-1}{2} \right\rfloor,$$

and the sign is taken, such that the following normalization holds:

$$\tilde{U}_d(0) \geq 0, \quad \left.\frac{d\tilde{U}_d(\nu_p)}{d\nu_p}\right|_{\nu_p=0} \geq 0, \quad d = 0, \dots, D-1. \tag{23}$$

Theorem 6.1 *The approximate DPS wave functions $\tilde{U}_d(\nu_p)$ converge to the DPS wave functions $U_d(\nu_p)$ as $\nu_{Dmax} \to 0$ and $M \to \infty$.*

Proof: We will prove the theorem by showing that both the approximate DPS wave function as well as the DPS wave function converge to the same function, namely the prolate spheroidal (PS) wave function $\psi_d(c,y)$, which are the continuous equivalent of the DPS wave functions [9].
Let $c>0$ be given and set

$$M = \left\lfloor \frac{c}{\pi \nu_{\mathrm{Dmax}}} \right\rfloor.$$

If $\nu_{\mathrm{Dmax}} \to 0$, then [6, Sec. 2.6]

$$\sqrt{\nu_{\mathrm{Dmax}}} U_d(\nu_p) \sim \psi_d(c, \nu_p/\nu_{\mathrm{Dmax}}). \tag{24}$$

We will now prove the theorem by showing that also the approximate DPS wave function $\sqrt{\nu_{\mathrm{Dmax}}}\tilde{U}_d(\nu_p)$ converge to $\psi_d(c,\nu_p/\nu_{\mathrm{Dmax}})$ for $\nu_{\mathrm{Dmax}} \to 0$.
We write

$$\sqrt{\nu_{\mathrm{Dmax}}}\tilde{U}_d(\nu_p) = \pm\sqrt{\frac{\lambda_d M}{2}} v^{(d)}_{m(\nu_p/\nu_{\mathrm{Dmax}})}. \tag{25}$$

If $\nu_{\mathrm{Dmax}} \to 0$, then [6, Sec. 2.6]

$$\pm\sqrt{\frac{\lambda_d M}{2}} v^{(d)}_{m(\nu_p/\nu_{\mathrm{Dmax}})} \sim \psi_d(c, \nu_p/\nu_{\mathrm{Dmax}}), \tag{26}$$

where the sign on the left hand side must be chosen, so that the normalizations on the PS wave functions [9] are fulfilled. This is however equivalent with the normalizations (23). □

Even in the finite case, the approximate DPS wave functions approximate the real DPS wave functions quite well, as it will be shown in the next section by numeric simulations. Therefore we can define

$$\tilde{\gamma}_d(\nu_p) := \frac{1}{\epsilon_d} e^{j\pi(M-1)\nu_l} \tilde{U}_d(\nu_p) \tag{27}$$

to approximately calculate the basis coefficients (21). For a given set of Doppler shifts $\{\nu_0,\ldots,\nu_{P-1}\}$, set $\gamma_{d,p} = \gamma_d(\nu_p), p = 0,\ldots,P-1$ and define the *approximate basis coefficients*

$$\tilde{\alpha}_d := \sum_{p=0}^{P-1} \eta_p \tilde{\gamma}_{d,p},\ d = 0,\ldots,D-1. \tag{28}$$

Finally we define the *approximate subspace representation*

$$\tilde{h}_m := \sum_{d=0}^{D-1} \tilde{\alpha}_d v^{(d)}_m. \tag{29}$$

Thus, we have found an algorithm for the efficient calculation of the subspace representation (16).

7. Approximation Error and Complexity Analysis

7.1 Approximation Error

In this subsection the mean square error of the approximate subspace representation (29),

$$\mathrm{MSE}_D = \mathcal{E}\left\{ \frac{1}{M} \sum_{m=0}^{M-1} |\tilde{h}_m - h_m|^2 \right\} \tag{30}$$

is analyzed. Using the triangle inequality,

$$\mathrm{MSE}_D \le \mathrm{bias}_D^2 + e_D^2, \tag{31}$$

where bias_D^2 is the squared bias of the subspace representation (16) (cf. Section 5) and e_D^2 is the approximation error of the approximate DPS wave functions,

$$e_D^2 = \mathcal{E}\left\{ \frac{1}{M} \sum_{m=0}^{M-1} |\tilde{h}_m - \hat{h}_m|^2 \right\}. \tag{32}$$

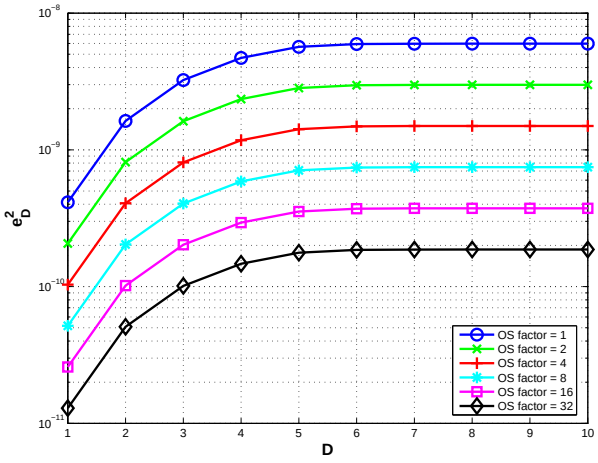

Figure 3: Mean square error e_D^2 of the approximate basis representation for different oversampling factors. The Doppler shifts ν_p are i.i.d. uniformly distributed.

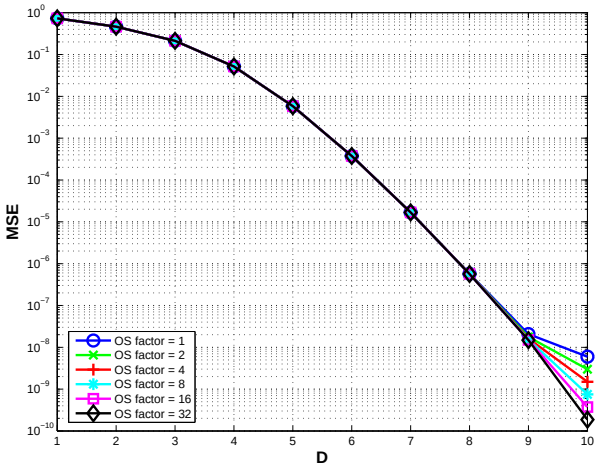

Figure 4: Overall error MSE_D of the approximate subspace representation of the channel model. The Doppler shifts ν_p are i.i.d. uniformly distributed.

Again, the approximation error of the multi-path model can be upper bounded by the approximation error of the single-path model, if it is assumed that the Doppler shifts ν_p as well as the attenuations η_p, $p = 0, \ldots, P-1$ are independently distributed. Using the fact, that $\sum_{m=0}^{M-1} |v_m^{(d)}|^2 = 1$, e_D^2 can further be bounded by

$$e_D^2 \leq \frac{1}{M} \sum_{d=0}^{D-1} \mathcal{E}\{|\gamma_d(\nu_p) - \tilde{\gamma}_d(\nu_p)|^2\}. \tag{33}$$

Theorem 6.1 suggests, that the approximation error e_D^2 gets smaller, as $\nu_{\mathrm{Dmax}} \to 0$ and $M \to \infty$, which is equivalent to OSF $\to \infty$ (cf. (14) and (15)). To show this dependence, we plot the upper bound of e_D^2 for different oversampling factors in Figure 3. The parameters are chosen according to Table 1 and the Doppler shifts ν_p are assumed to be i.i.d. uniformly distributed. We observe, that the upper bound is below the accuracy of a fixed-point implementation. Even for an oversampling factor of 1, the error stays below the numerical precision of $2^{-15} \approx 3 \cdot 10^{-5}$.

The overall error MSE_D (30) is plotted in Figure 4. It can be seen, that the dominating error in the whole algorithm is the bias of the subspace representation. The approximation error introduced through the approximation of the basis coefficients is marginally small and does not influence the precision on a fixed point processor.

Another important issue is the resolution or quantization of (27) with respect to ν_p. Since $m(\nu_p/\nu_{\mathrm{Dmax}})$ can only take integer values, $\tilde{U}_d(\nu_p)$ is a step function. The step width is given by

$$s = 2\nu_{\mathrm{Dmax}}/M.$$

For the example given in Section 5, $s \approx 6.13 \cdot 10^{-11}$. However, when assigning 16 bit to ν_{Dmax} on a fixed-point processor, the maximal resolvable step width is only $s' \approx 2.48 \cdot 10^{-10}$, i. e. (27) cannot be fully resolved anyway.

7.2 Complexity

In this subsection the computational complexity of the algorithm to compute the approximate subspace representation (29) is evaluated and compared to the algorithm described in the appendix of [7], which is an enhanced version of Zheng's sum of sinusoids (SoS) model [2].

The calculation of the DPS sequences is not taken into account, since this can be done offline. The computational complexity is evaluated theoretically, counting the number of operations as well as numerically, measuring the run time of a Matlab implementation on an AMD Athlon machine with 1.26GHz clock speed and 512MB RAM.

For the operations count, we use the number of complex multiplications (CM), evaluations of the complex

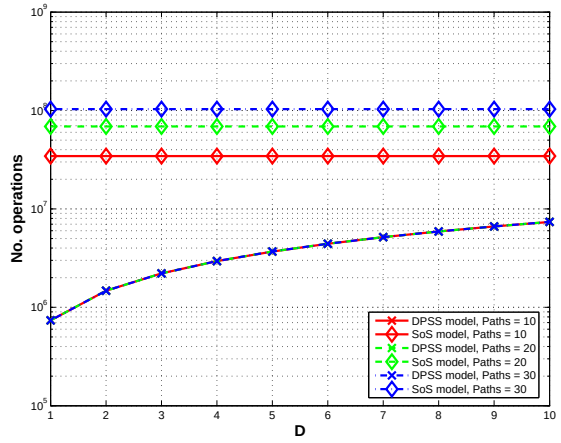

Figure 5: Number of operations and execution time respectively of the sum-of-sinusoids model compared to the approximate subspace representation (DPSS) plotted over the subspace dimension D for different number of paths.

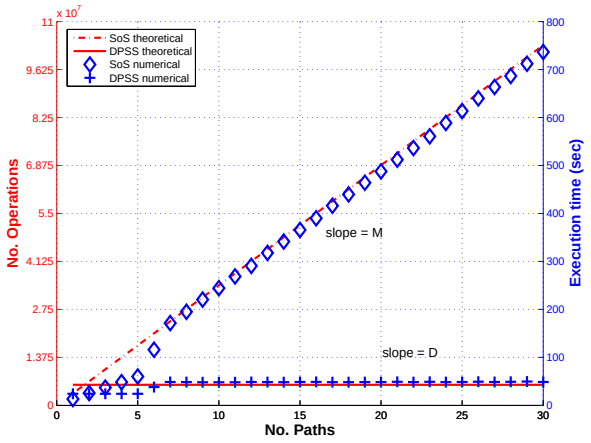

Figure 6: Number of operations and execution time respectively of the sum-of-sinusoids model compared to the approximate subspace representation (DPSS) plotted over the number of paths for a fixed subspace dimension of $D = 8$.

exponential (CE), and the number of complex dotproducts of length K (CDOT(K)),

$$\sum_{k=0}^{K-1} x_k y_k.$$

It is fruitful to count the number of dotproducts separately, because digital signal processors are especially optimized for such operations. For example, on a Texas Instruments C6416 DSP, it can be evaluated in $2K + 15$ cycles [10]. On the same processor, the costs for a CE is 12 cycles and the costs for a CM is 6 cycles.

The approximate basis coefficients $\tilde{\alpha}_d$ can be calculated in

$$C_{\tilde{\alpha}} = PD(1\,\mathrm{CE} + 2\,\mathrm{CM}) + D\,\mathrm{CDOT}(P)$$

operations, where the first term accounts for the calculation of the coefficients $\tilde{\gamma}_{d,p}$ in (27), and the second term for the calculation of $\tilde{\alpha}_d$ in (28). In total, for the evaluation of the approximate subspace representation of the channel (29),

$$C_{\mathrm{DPSS}} = D\mathrm{CDOT}(P) + C_{\tilde{\alpha}}$$

operations are required.

On the other hand, the sum of sinusoids algorithm (4) needs

$$C_{\mathrm{SoS}} = MP\,\mathrm{CE} + M\,\mathrm{CDOT}(P)$$

operations for every block of length M.

The number of operations C_{DPSS} and C_{SoS} are plotted over the subspace dimension D for different number of paths P in Figure 5. The numerical runtime evaluations of the Matlab implementations of both models match very well with the theoretical results and are thus not shown here for brevity. It can be seen, that for a subspace dimension of $D = 8$ and $P = 20$ paths a magnitude in complexity is saved.

In Figure 6, the number of operations C_{DPSS} and C_{SoS} as well as the execution time (in seconds) are plotted over the number of paths P for a fixed subspace dimension of $D = 8$. This is the dimension needed for an accurate implementation on a 16 bit fixed-point processor (cf. Section 5). It can be seen, that the the complexity of the sum-of-sinusoids implementation increases with slope $M = 245760$ with increasing number of paths. On the other hand, the complexity of the new subspace based implementation increases only with slope $D = 8$. Again, the theoretical results match the numerical results quite well.

The lesser complexity comes at the cost of more memory storage and memory accesses. However, the memory accesses in the algorithm are perfectly linear and if the cache is optimally used, the access latency can be neglected. The storage requirements can be quite high. For the given system the DPS sequences need 1.875 Mbyte storage.

8. Conclusions

We have presented a low-complexity algorithm for the simulation of time-variant flat-fading channels, which is very attractive for the implementation on real-time hardware channel simulators. The subspace representation is independent of the number of propagation paths. By adjusting the dimension of the subspace it is possible to trade complexity for accuracy. For a given numerical precision of, e. g. 16 bits, the required subspace dimension is as little as seven and the complexity can be reduced by one order of magnitude.

Future work includes an extension of the proposed schemes to frequency selective fading and multiple-input multiple-output channels.

Acknowledgements

This work was funded by the Wiener Wissenschafts- Forschungs- und Technologiefonds (WWTF) in the ftw. project "Math+MIMO" (I2).

Appendix—Bias of the subspace representation

To analyze the square bias of the subspace representation (19) analytically, we start with the single-path model

$$g_m = e^{j2\pi\nu_p m}, \quad \hat{g}_m = \sum_{d=0}^{D-1} \gamma_{d,p} v_m^{(d)}.$$

Assuming that the Doppler shift ν_p is drawn from a uniform distribution, we get [11]

$$\text{bias}^2_{D,\text{single}} = \mathcal{E}\left\{ \frac{1}{M} \sum_{m=0}^{M-1} |g_m - \hat{g}_m|^2 \right\} = \frac{1}{2M\nu_{Dmax}} \sum_{d=D}^{M-1} \lambda_d.$$

Since λ_d decays exponentially with d, $\text{bias}^2_{D,\text{single}}$ also decays exponentially with the subspace dimension D.

In the multi-path model (4), the square bias (19) also depends on the joint distribution of the Doppler shifts ν_p and the attenuations η_p, $p = 0, \ldots, P-1$. Assuming they are independent, and that $\mathcal{E}\{|\eta_l|^2\} = \frac{1}{P}$, we get

$$\begin{aligned}
\text{bias}^2_{D,\text{multi}} &= \mathcal{E}\left\{ \frac{1}{M} \sum_{m=0}^{M-1} |h_m - \hat{h}_m|^2 \right\} \\
&= \mathcal{E}\left\{ \frac{1}{M} \sum_{m=0}^{M-1} \left| \sum_{p=0}^{P-1} \eta_p (g_m - \hat{g}_m) \right|^2 \right\} \\
&\le \mathcal{E}\left\{ \frac{1}{M} \sum_{m=0}^{M-1} \sum_{p=0}^{P-1} |\eta_p|^2 |(g_m - \hat{g}_m)|^2 \right\} \\
&= \sum_{p=0}^{P-1} \mathcal{E}\{|\eta_p|^2\} E_D^{(1)} \\
&= \text{bias}^2_{D,\text{single}}.
\end{aligned}$$

It can be seen, that the square bias for the multi-path model is *upper bounded* by the square bias of the single-path model.

The same argument can be used to show the the MSE of the approximate subspace representation of the multi-path model (30) can be upper bounded by the MSE of the subspace representation of the single-path model.

References

[1] W.C. Jakes, *Microwave Mobile Communications*, Wiley, 1974.

[2] Y. R. Zheng and C. Xiao, "Simulation models with correct statistical properties for Rayleigh fading channels," *IEEE Trans. Commun.*, vol. 51, no. 6, pp. 920–928, June 2003.

[3] L. M. Correia, *Wireless Flexible Personalised Communications*, Wiley, 2001.

[4] H. Hofstetter and G. Steinböck, "A geometry based stochastic channel model for MIMO systems," in *ITG Workshop on Smart Antennas*, Munich, Germany, January 2004.

[5] F. Kaltenberger, G. Steinböck, R. Kloibhofer, R. Lieger, and G. Humer, "A multi-band development platform for rapid prototyping of mimo systems," in *ITG Workshop on Smart Antennas*, Duisburg, Germany, April 2005.

[6] D. Slepian, "Prolate spheroidal wave functions, Fourier analysis, and uncertainty - V: The discrete case," *The Bell System Technical Journal*, vol. 57, no. 5, pp. 1371–1430, May-June 1978.

[7] T. Zemen and C. F. Mecklenbräuker, "Time-variant channel estimation using discrete prolate spheroidal sequences," *IEEE Trans. Signal Processing*, vol. 53, no. 9, pp. 3597–3607, September 2005.

[8] F. Kaltenberger, K. Freudenthaler, S. Paul, J. Wehinger, C.F. Mecklenbräuker, and A. Springer, "Throughput enhancment by cancellation of synchronization and pilot channel for UMTS high speed downlink packet access," in *Proceedings of the SPAWC*, New York, USA, June 2005, pp. 580–584.

[9] D. Slepian and H. O. Pollak, "Prolate spheroidal wave functions, Fourier analysis, and uncertainty - I," *The Bell System Technical Journal*, vol. 40, no. 1, pp. 43–64, January 1961.

[10] Texas Instruments, *TMS320C64x DSP Library Programmer's Reference*, October 2003.

[11] Paolo Tilli, *Fast Reliable Algorithms for Matrices with Structure*, chapter 6, SIAM, 1999.